Recent progress of room temperature THz sources based on nonlinear frequency mixing in quantum cascade lasers

M. Razeghi [a)], Q. Y. Lu, N. Bandyopadhyay, S. Slivken, Y. Bai

Center for Quantum Devices, Department of Electrical Engineering and Computer Science, Northwestern University, Evanston, Illinois 60208

ABSTRACT

We present the recent development of high performance compact THz sources based on intracavity nonlinear frequency mixing in mid-infrared quantum cascade lasers. Significant performance improvements of our THz sources in the spectral purity, frequency coverage as well as THz power are achieved by systematic optimizing the device's active region, waveguide, phase matching scheme, and chip bonding strategy. Room temperature single-mode operation in a wide THz spectral range of 1-4.6 THz is demonstrated from our Čerenkov phase-matched THz sources with dual-period DFB gratings. High THz power up to 215 μW at 3.5 THz is demonstrated via epi-down mounting of our THz device. The THz power is later scaled up to mW level by increased the mid-IR power and conversion efficiency. The rapid development renders this type of THz sources promising local oscillators for many astronomical and medical applications.

Keywords: terahertz, quantum cascade lasers, difference frequency generation, distributed feedback

1. INTRODUCTION

Terahertz (THz) radiation (v ~ 0.1-10 THz) falls in between infrared radiation and microwave radiation in the electromagnetic spectrum. Many common materials and living tissues are semitransparent and have 'terahertz fingerprints', permitting them to be imaged, identified and analyzed. Due to non-ionizing properties, terahertz radiations are safe for screening application. Nevertheless, the technology for generating and manipulating it is still in its infancy and is a subject of active research [1]. Room temperature THz sources with low cost, compact size, high power, and wide frequency tunibility are always desired for the wide applications. The GaAs-based THz quantum cascade lasers (QCLs) have emerged as the most powerful semiconductor THz sources in the 2-5 THz range, however, cryogenic cooling is still a necessity. [2,3]. On the other hand, the THz source based on intracavity difference frequency generation (DFG) in mid-IR QCL has gained considerable progress in the past few years [4-9]. This type of THz source is free from the temperature limitation suffered by the THz QCLs based on direct optical transition, and ideally its working temperature is only limited by the mid-IR QCL which can work well even above 100 °C [10]. It not only shares the common features of the mid-IR QCLs which are semiconductor lasers, room temperature operation, low cost, small size, and high efficiency, but also carries the potentials of delivering THz emission with high power in a wide frequency range.

The systematic optimization starts with the dual-core design [6] based on single phonon resonance structure for high efficiency and broad gain operation. Composite distributed-feedback (DFB) grating with dual period component [5]

[a)] email: razeghi@eecs.northwestern.edu

Image Sensing Technologies: Materials, Devices, Systems, and Applications, edited by Nibir K. Dhar, Achyut K. Dutta, Proc. of SPIE Vol. 9100, 91000H · © 2014 SPIE · CCC code: 0277-786X/14/$18 · doi: 10.1117/12.2054324

is introduced to purify and tune the mid-IR as well as the THz spectra. Čerenkov phase-matching scheme [6] is used to enhance the THz outcoupling efficiency. Epi-down bonding on patterned submount is used to improve the heat dissipation and uniform electrical current injection. After the first demonstration of room temperature single-mode operation THz emission based on DFG in QCLs at 4 THz, the frequency coverage is upgraded to 1-4.6 THz with average side mode suppression ratio (SMSR) up to 30 dB by using Čerenkov phase-matching scheme [6]. Even higher THz power was obtained from the collinearly modal-phase matched THz QCL sources at 4 THz, with THz output power up to 65 μW and SMSR of 40 dB [7]. THz power is later increased to 215 μW by epi-down bonding of the Čerenkov phase-matched device [9]. Further scaling up the THz power with mid-IR power and conversion efficiency by higher doping in the active region and broader device area, THz power to mW level is recently demonstrated. The rapid developments in power, efficiency, and spectral range render this type of THz source a promising local oscillator for many astronomical and medical applications.

2. DUAL-PERIOD COMPOSITE DFB GRATING

In a typical multimode Fabry-Pérot (FP) cavity, the light intensity spreads out among different mid-IR frequencies, and the total power is the sum over many small W_i components. As such, the product W_iW_j will be small and the THz spectrum will rather broad ($\Delta\nu$ ~ 0.5-1 THz). In order to purify and tune the THz spectrum, all the mid-IR power needs to be concentrated on the two mid-IR frequencies with single mode operation, and their frequency positions need to be controllable and tunable. The most straightforward way to this end is to use the integrated dual-period DFB grating to purify and tune the mid-IR spectra. While the design strategy of dual-period DFB grating shares some similarity to the single-period DFB like sufficient coupling strength for single mode operation, balancing the coupling strength, waveguide loss, and modal gain of the two grating components is of special importance.

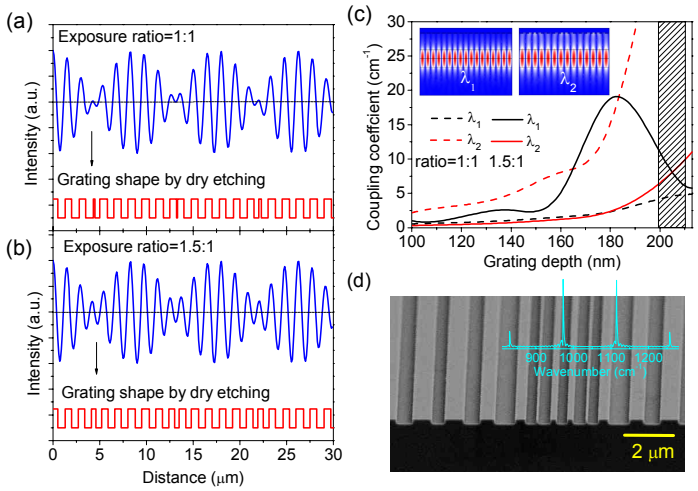

FIG. 1. Superpositioned HL interferograms with exposure dose ratio of 1:1 (a) and 1.5:1 (b) and the truncated square gratings after dry etching. (c) Coupling coefficients of the truncated gratings in (a) and (b) with different grating depths. The shaded region is the targeted grating depth. The insets in (c) are two eigenmodes for the dual-period grating. (d) SEM image of a dual-period grating after dry etching. Inset: Fourier analysis of the corresponding gratings

Double exposure holographic lithography (HL) or electron-beam (e-beam) lithography has used to define the dual-period DFB grating for both mid-IR and THz spectral purifications. Figure 1(a) shows the simulated superpositioned HL interferograms with equal-dose double exposures. As it is difficult to accurately reproduce the

photo resist profile with anisotropic dry etching processing, the pattern was simply truncated into binary-equivalent square-shaped structures when transferred into SiO_2 mask, as shown in Fig. 1(a). Figure 1(c) shows the calculated coupling coefficients (κ_1 for λ_1 and κ_2 for λ_2) for the case of equal exposure intensity. Clearly, κ_1 is much smaller than κ_2. This is because the longer wavelength λ_2 has a more expanded mode profile (see the inset of Fig. 1(c)) and has a stronger interaction with the surface gratings than the shorter wavelength λ_2. To obtain similar coupling coefficients, the grating shape is reconstructed by changing the dose ratio of the two exposures with a similar strategy as in Ref. 27. The HL interferogram with a dose ratio of 1.5:1, the truncated grating profile are shown in Fig. 1(b). Around a grating depth of 200 nm (shaded region in Fig. 1(c)), the coupling coefficients of these two wavelengths are similar (6~10 cm^{-1}). This design offers sufficient coupling strength for 2-3 mm cavities with high-reflection (HR) coatings. For the case of e-beam lithography, the grating profile will be similar to the superpositioned interferogram of the two rectangular waves, as shown in Fig. 1(d). Double e-beam exposure with the same exposure doses is used for two gratings with different period components, which naturally balances the coupling strengths for the two wavelengths via their different grating duty cycles. The Fourier analysis of the extrapolated grating shape from the scanning electron microscope SEM picture shown in the inset of Fig. 1(d) gives two distinct peaks with a THz energy spacing at 4 THz. The other two satellite peaks with the same energy spacing away from the two main peaks correspond to the high-order Fourier series of the grating shape.

3. EPI-DOWN BONDING OF ČERENKOV THZ DEVICES

Despite the higher conversion efficiency, the THz power of the Čerenkov phase-matched device was lower than the modal phase-matched device because of a poorer heat removal mechanism due to the epilayer-up mounting and 350 μm thick substrate, and a less efficient current injection scheme due to the single-side current injection through a thin layer of bottom contact. Figure 2(a) and (b) show the temperature and electrical potential distributions of an epilayer-up mounted QCL with an asymmetric contact pattern (single-sided current injection) near the front facet. The x, y, and z directions are the lateral, longitudinal, and growth directions, respectively. The polished angle of the facet is set to be 30°. Clearly, the Čerenkov device suffers severely from both thermal and electrical issues, as the heat near the front facet is not effectively dissipated and the non-uniform electrical distribution across the active region induces non-uniform current injection with the electrical field varying over 2-4 kV/cm.

To address these two issues, we design and demonstrate double-sided current injection and epilayer-down mounting on a submount. Fig. 2(c) and (d) show the temperature and electrical potential distributions of a device with epilayer-down mounting to a diamond submount. The heat dissipation is improved significantly and the electrical distribution is much more uniform with electrical field variation less than 0.5 kV/cm in the x-z plane of the active region. In the experiment, AlN or diamond submounts are prepared with the patterns corresponding the contacts of the device for epi-down bonding. Figure 2(e) is the schematic of an epi-down mounted Čerenkov THz device.

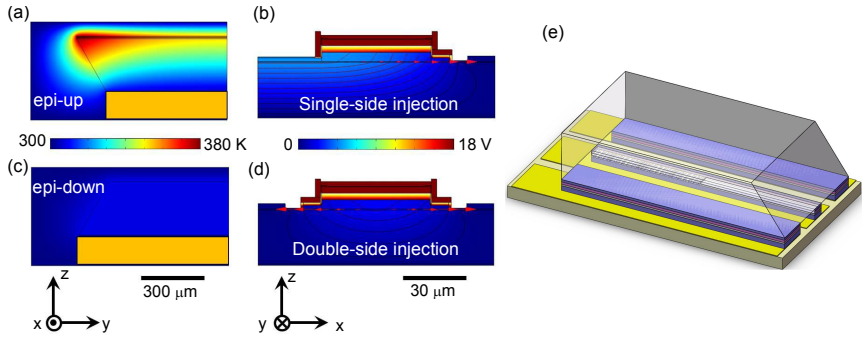

Fig. 2. Temperature and electrical potential distributions of devices with epilayer-up (a)-(b) and epilayer-down mounting schemes (c)-(d). The lines and arrows in (b) and (d) denote the contour lines of the electrical potential and the current flow. Current injection is single-sided in (b) and double-sided in (d). (e) Schematic of an epi-down mounted Čerenkov THz device.

4. DEVICE CHARACTERIZATIONS

The QCL structure is based on the single phonon resonance (SPR) dual-core structure with the lattice-matched $In_{0.53}Ga_{0.47}As/In_{0.52}Al_{0.48}As$ laser core grown by gas-source molecular beam epitaxy on a semi-insulating InP substrate. The waveguide structure consists of a 250-nm InP bottom contact (Si, ~1×10^{18} cm^{-3}), a 100-nm InGaAs etching stop layer (Si, ~1×10^{18} cm^{-3}), a 3-5-μm InP buffer(Si, ~1.5×10^{16} cm^{-3}), dual core active region with average doping of 5.3×10^{16} cm^{-3}, a 3.2-3.5-μm InP cladding layer (Si, ~1.5×10^{16} cm^{-3}), and a 0.2-μm InP cap layer (Si, ~5×10^{18} cm^{-3}). The sample is processed into double-channel geometries with a ridge width of 20 μm. The 1.5-mm long DFB section is patterned with a dual-period grating within a 3-mm long laser cavity. A row of devices with dual-period DFB gratings spanning a THz frequency range from 1.0 to 4.6 THz are defined by electron beam lithography. The grating is defined on the InP cap layer with a depth of 0.2 μm. The substrate near the front facet has been polished at 25° with respect to the normal cleavage plane without damaging the mid-IR facet in order to collect the THz signal which satisfies the Čerenkov phase-matching scheme.

The mid-IR output power in pulsed mode operation with 1% duty cycle was measured using a calibrated thermopile detector. The mid-IR spectra were taken in rapid scan mode at a resolution of 0.125 cm^{-1} from a Bruker Fourier transform infrared (FTIR) spectrometer equipped with a mid-IR DTGS detector. The power-current-voltage (*P-I-V*) characterizations of the epi-down bonded devices are shown in Fig. 3(a). The device exhibits stable dual-wavelength operation at λ_1 =9.26 μm and λ_2 =10.4 μm in the working current range, as shown in Fig. 3(b). The mid-IR frequency difference corresponds to 117 cm^{-1} (~3.5 THz).

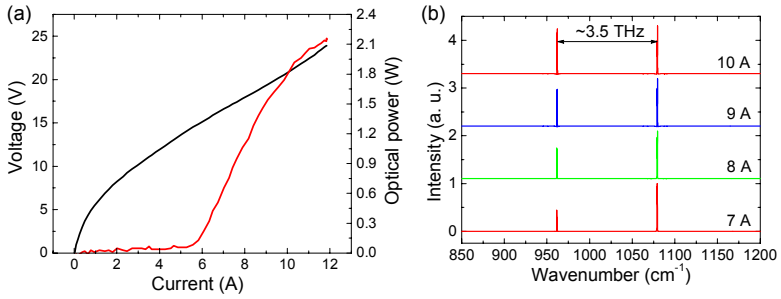

Fig. 3. Mid-IR P-I-V characterizations at different currents for the epil-up and -down mounted devices. Inset: lasing spectra at 10 A for the epi-down mounted device.

Single mode operations from 1.0 to 4.6 THz are demonstrated from a array of THz devices as shown in Fig. 4(a), with a frequency step-tuning range ($\Delta\nu$) of 3.6 THz and a mean SMSR above 30 dB. This range represents 1.28 times that of the central frequency. For each of the device, the THz spectral position is pretty stable with respect to the temperature or current changes. The average current tuning rate is about 1 GHz/A and the linewidth is about 6-8.6 GHz, which is mainly limited by the resolution of the FTIR spectrometer (0.125 cm^{-1}). Much wider, continuous tuning can be achieved by employing the dual-section sampled grating design [11].

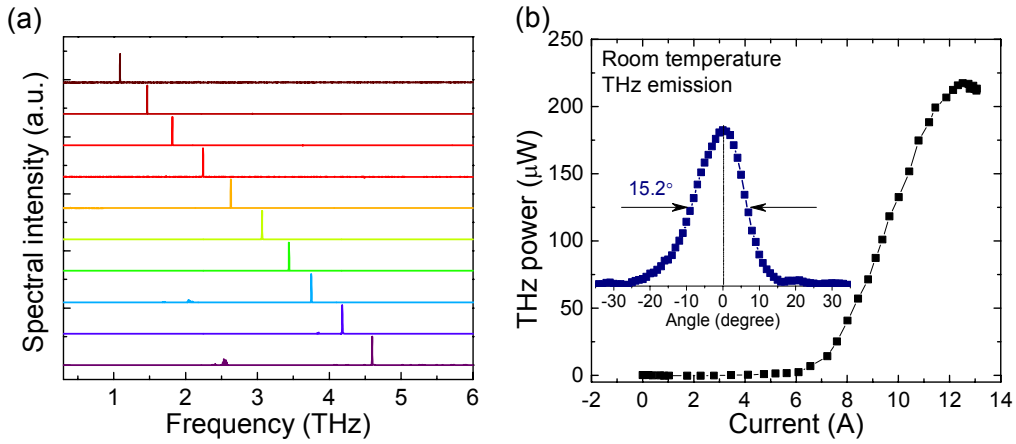

Fig. 4 THz power as a function of current for the devices with various mounting and polishing strategies. 'Polishing' indicates the polishing into the active region area. Fig. 4. (a) THz spectra of the epilayer-down mounted device at different working currents. (b) THz far fields of the epilayer-down mounted device in vertical and lateral directions.

For the epi-down bonded device, the InP substrate is exposed. Therefore, THz power can be further enhanced by THz anti-reflection (AR) coating. Several materials have been employed as the THz AR coating, such as SiO_2, Parylene, and low-density Polyethylene.[12,13] Here SU-8 photoresist is used for its simplicity. The experimental results shows that a maximum transmission of ~87% can be obtained for SU-8 coating with an optimal coating thickness ~11 μm. The SU-8 photoresist is then spin coated on the mounted device, and baked and cured. The coating thickness is controlled by the spin rate. The THz powers after the SU-8 coating is shown in Fig. 3. The power is enhanced by 17.5% to 215 μW. Ideally, with the low-loss coatings, such as SiO_2, or low-density Polyethylene, power enhancement above 40% can be achieved. THz far fields in the lateral and vertical directions for the epi-down mounted device at a working currents are shown in the inset of Fig. 4(b). The device exhibits no beam steering and single-lobed beam distributions in both directions with a full width at half maximum (FWHM) of 15.2° and 38°, respectively. The THz beam peaks at 0° in both directions.

For our epi-down bonded THz device in pulsed mode operation, the internal heating is negligible, the THz power can be further scaled up by increasing the mid-IR power and conversion efficiency. A wafer with two 30-stage SPR structures, a higher doping (~7 $\times 10^{16}$ cm^{-3}) in the active region, and a thinner cladding layer of 3 μm for strong surface DFB coupling is processed into 24 μm wide ridge waveguide and cleaved into 3 mm long laser bar. THz peak power is further scaled up to 1.4 mW in pulsed mode by increasing the mid-infrared power through increasing the active region doping and device area. Note that given the limited substrate thickness and the Čerenkov angle θ_C =22°, only 1/3 of intracavity generated THz power can be coupled out directly from the 3 mm long cavity.

Considering that the back-travelling THz is not collected, total THz power above 5 mW may has been generated in the cavity. Optimization in the waveguide design is able to enhance the THz output significantly.

In conclusion, we have demonstrated widely tuned, single mode operation, high power, high efficiency THz QCL sources with a Čerenkov phase-matching scheme by applying the epi-down mounting strategy. Consistent optimization in the waveguide, active region, phase matching scheme, and device package, mW THz power is achieved from this type of compact device at room temperature.

5. ACKNOWLEDGEMENTS

This work is partially supported by the National Science Foundation under grants ECCS-1231289 and ECCS-1306397. The authors would also like to acknowledge the encouragement and support of Dr. K.K. Law from the Naval Air Warfare Center, Dr. T. Manzur from the Naval Undersea Warfare Center, and Dr. N. Dhar from the Defense Advanced Research Projects Agency.

REFERENCES

[1]. Tonouchi, M., "Cutting edge terahertz technology," Nat. Photonics 1, 97-105 (2007).

[2]. Köhler, R., Tredicucci, A., Beltram, F., Beere, H. E., Linfield, E. H., Davies, A. G., Ritchie, D. A., Iotti, R. C., and Rossi, F., "Terahertz semiconductor-heterostructure laser," Nature 417, 156 (2002).

[3]. Fathololoumi, S., Dupont, E., Chan, C.W. I., Wasilewski, Z. R., Laframboise, S. R., Ban, D., Mátyás, A., Jirauschek, C., Q. Hu, and Liu, H. C., "Terahertz quantum cascade lasers operating up to ~200 K with optimized oscillator strength and improved injection tunnelling," Optics Express, 20, 3866 (2012).

[4]. Belkin, M. A., Capasso, F., Xie, F., Belyanin, A., Fischer, M., Wittmann, A., and Faist, J., "Room temperature terahertz quantum cascade laser source based on intracavity difference-frequency generation," Appl. Phys. Lett., 92, 201101 (2008).

[5]. Lu, Q. Y., Bandyopadhyay, N., Slivken, S., Bai, Y., and Razeghi, M., "Room temperature single-mode terahertz sources based on intracavity difference- frequency generation in quantum cascade lasers," Appl. Phys. Lett. 99, 131106 (2011).

[6]. Lu, Q. Y., Bandyopadhyay, N., Slivken, S., Bai, Y., and Razeghi, M., "Widely tuned room temperature terahertz quantum cascade laser sources based on difference-frequency generation," Appl. Phys. Lett. 101, 251121 (2012).

[7]. Lu, Q. Y., Bandyopadhyay, N., Slivken, S., Bai, Y., and Razeghi, M., "High performance terahertz quantum cascade laser sources based on intracavity difference frequency generation," Optics Express 21, 968 (2013).

[8]. K. Vijayraghavan, Y. Jiang, M. Jang, A. Jiang, K. Choutagunta, A. Vizbaras, F. Demmerle, G. Boehm, M. C. Amann, and M. A. Belkin, Nature Commun. 4, 2021 (2013).

[9]. Lu, Q. Y., Bandyopadhyay, N., Slivken, S., Bai, Y., and Razeghi, M., " Room temperature terahertz quantum cascade laser sources with 215 μW output power through epilayer-down mounting " Appl. Phys. Lett. 103, 011101 (2013).

[10]. Bai, Y., Bandyopadhyay, N., Tsao, S., Slivken, S., and Razeghi, M., "Room temperature quantum cascade lasers with 27% wall plug efficiency," Appl. Phys. Lett., 98, 181102 (2011).

[11]. Slivken, S., Bandyopadhyay, N., Tsao, S., Nida, S., Bai, Y., Lu, Q.Y., and Razeghi, M., Appl. Phys. Lett. "Sampled grating, distributed feedback quantum cascade lasers with broad tunability and continuous operation at room temperature," 100, 261112 (2012).

[12]. Xu, J., Hensley, J. M., Fenner, D. B., Green, R. P., Mahler, L., Tredicucci, A., Allen, M. G., Beltram, F., Beere, H. E., and Ritchie, D. A., " Tunable terahertz quantum cascade lasers with an external cavity," Appl. Phys. Lett. 91, 1 (2007).

[13]. Lee, A. W. M., Qin, Q., Kumar, S., Williams, B. S., Hu, Q., and Reno, J. L., " Tunable terahertz quantum cascade lasers with external gratings," Opt. Lett. 35, 910 (2010).